4A.6 POLARIMETRIC CHARACTERISTICS OF MELTING HAIL AT S AND C BANDS

A. Ryzhkov[(1)], S. Ganson[(1)], A. Khain[(2)], M. Pinsky[(2)], and A. Pokrovsky[(2)]
(1) CIMMS/OU and NOAA/NSSL, Norman, Oklahoma, USA
(2) Hebrew University of Jerusalem, Jerusalem, Israel

1. INTRODUCTION

Polarimetric method for hail detection is based on the assumption that differential reflectivity Z_{DR} of hail is low due to almost random orientation of hailstones, and the combination of low Z_{DR} and high reflectivity factor Z points to the presence of hail (Bringi and Chandrasekar 2001). Limited validation studies (e,g., Heinselman and Ryzhkov 2006; Depue et al. 2007) have demonstrated good overall skills of the method at S band. However, several practically important issues regarding detection of hail and determination of its size at different radar wavelengths remain to be resolved. These include

(1) Estimation of maximal hail size. The most recent version of hydrometeor classification algorithm (HCA) for polarimetrically upgraded WSR-88D radars implies detection of "rain mixed with hail" (Park et al. 2009) and does not distinguish between large and small hail.

(2) Separation of hail and rain in the mixture. Hail is commonly mixed with rain below the freezing level. Larger hailstones with original sizes exceeding 20 – 30 mm do not entirely melt on the way to the ground and their polarimetric signatures may be overwhelmed by the ones caused by rain originating from smaller size hailstones and graupel. This also necessitates taking into account the height of the radar sampling volume with respect to the freezing level.

(3) Adaptation of the hail detection procedure originally developed and validated at S band for the use at shorter radar wavelengths. There is growing evidence that intrinsic Z_{DR} of hail/rain mixture (after correction for differential attenuation) at C band is noticeably higher than the one at S band (Ryzhkov et al. 2007).

(4) Anomalously high attenuation / differential attenuation frequently reported at C band and their possible relation to the presence of hail (e.g., Tabary et al. 2008). Such differential attenuation in "hotspots" is difficult to correct and it has very strong impact on the magnitude of Z_{DR} and reliability of hail detection at C band.

This study is an attempt to develop possible approaches to address these four issues and to interpret observed polarimetric signatures of hail at S and C bands by examining two microphysical models of melting hail.

2. MODEL DESCRIPTION

Similar to earlier works of Aydin and Zhao (1990), Aydin and Giridhar (1991), and Vivekanandan et al. (1990), one of the models (Model 1) makes use of the Rasmussen and Heymsfield (1987) study of the physics of individual melting hailstone. It assumes certain distribution of graupel / hail at the freezing level and follows the change of the size distribution of partially melted ice particles / raindrops and the corresponding polarimetric radar variables as hydrometeors (totally or partially melted) reach the ground. This is a steady state 1D model which takes into account shedding of excessive water from the surface of melting hailstones but does not allow for interactions / collisions between the particles of different original sizes.

The second model (Model 2) is the 2D nonhydrostatic mixed-phase spectral bin Hebrew University of Jerusalem Cloud Model (HUCM) (e.g., Khain et al. 2004). The model contains 7 classes of hydrometeors and each class is represented by size distribution functions in 43 size bins. As opposed to Model 1, this model explicitly describes both generation and melting of hail and takes into account all sorts of interaction between hydrometeors.

The output of both models is converted to the vertical profiles and fields of radar reflectivity Z, differential reflectivity Z_{DR}, specific differential phase K_{DP}, cross-correlation coefficient ρ_{hv}, specific attenuation A_h, and specific differential attenuation A_{DP} at S and C bands as partially described in Ryzhkov et al. (2009) and Kumjian and Ryzhkov (2008). The scatterers are modeled as uniformly filled oblate spheroids with symmetric Gaussian distribution of orientations with respect to the vertical and variable width of the canting angle distributions σ. Aspect ratio and parameter σ of mixed-phase hydrometeors linearly depend on mass water content which changes across size spectra. The combination of simple Rayleigh formulas and T-matrix codes is used for computation of backward and forward scattering amplitudes (see details in Ryzhkov et al. 2009).

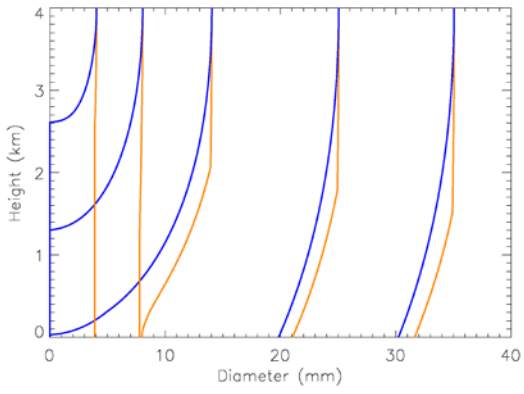

Fig. 1 Dependencies of diameters of melting hailstones and their ice cores on height. Red curves depict total diameter of melting particles, blue curves – diameter of ice cores

Corresponding author address: Alexander Ryzhkov, CIMMS/NSSL, Norman, Oklahoma
e-mail: Alexander.Ryzhkov@noaa.gov

3. SIZE DEPENDENCIES OF RADAR VARIABLES

Smaller ice particles melt completely, whereas larger ones can reach the ground with only minor change in the size of their ice core. The dependencies of diameters of melting hailstones and their ice cores on height estimated with Model 1 are illustrated in Fig. 1. The computations have been performed assuming that the freezing level is at 4 km, temperature lapse rate is 6.5 deg/km, relative humidity is 100%, and original density of ice particles is equal to the one of solid ice (0.92 g/cm^3).

Fig. 1 shows that hailstones with initial diameters (i.e., diameters aloft) less than 14 mm melt completely before reaching the ground, whereas ice cores of much bigger hailstones remain rather large. Shedding of water from the surface of larger melting hailstones causes reduction of their mass and diameter.

At each height below the freezing level, mass water fraction f_m is equal to 1 for totally melted particles and gradually decreases with size of partially melted graupel / hail (Fig. 2). Once the size of maximal raindrop

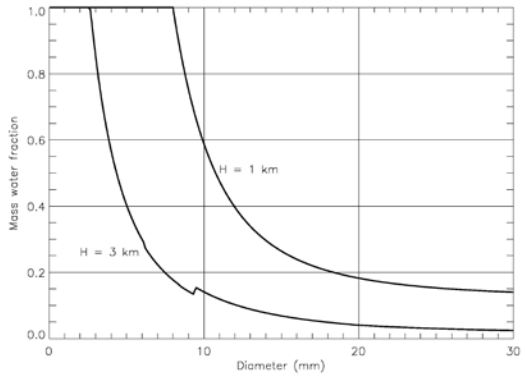

Fig. 2 Distribution of mass water fraction across size spectrum at two different heights.

resulting from melting hail reaches 8 mm (at about 1.3 km height), the f_m – D dependence does not change. This is a consequence of the shedding condition (Rasmussen and Heymsfield 1987)

$$M_w = 0.268 + 0.1389 M_i \quad , \qquad (1)$$

where M_i and M_w are masses (in g) of ice core and water coating which melting hailstone is capable to retain before shedding occurs.

Because dielectric constant, shape, and the width of the canting angle distribution of melting particles are determined by their size and mass water fraction, the dependencies of radar variables on particle size for monodisperse distributions do not change with height H if H < 1.3 km. These dependencies are displayed in Fig. 3. It is important that differential reflectivity of melting hailstones (D > 8 mm) at both radar wavelengths is lower than Z_{DR} of large raindrops which can be as high as 8 dB for the resonance raindrop size of about 6 mm at C band. This is primarily due to more spherical shape, lower water content, and more chaotic orientation of melting hailstones. Thus, according to Model 1, melting hailstones with sizes exceeding 8 mm generally tend to decrease Z_{DR} if mixed with raindrops characterized by higher intrinsic values of Z_{DR}. On the other hand, normalized values of A_h and A_{DP} of melting

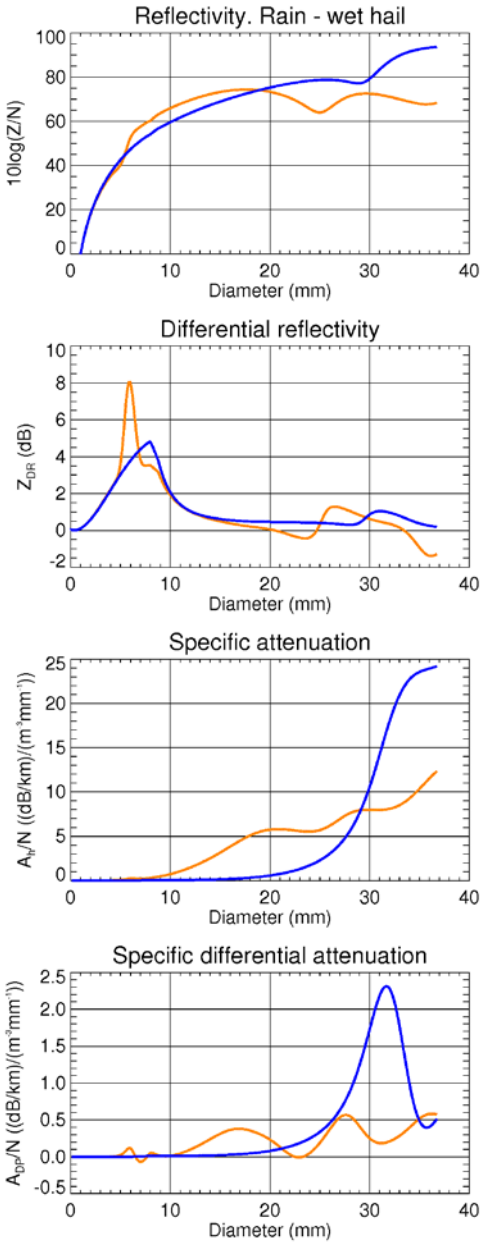

Fig. 3. Size dependencies of Z/N, Z_{DR}, A_h/N, and A_{DP}/N at heights below 1.3 km. N is concentration of mondisperse particles; blue and red curves are for S and C bands respectively.

hailstones are generally much higher than the ones associated with raindrops.

4. SIZE DISTRIBUTIONS OF MELTING HAILSTONES

The advantage of Model 1 is that it allows studying the impact of size distribution of graupel / hailstones aloft on vertical profiles of radar variables in the most direct and straightforward way. In situ measurements of size distribution of ice particles aloft in hailstorms often reveal bi-exponential type of particle spectra with different slopes for graupel-size and hail-size hydrometeors (Smith et al. 1976; Spahn and Smith 1976). In our simulations with Model 1, we prescribe bi-exponential size distribution of graupel / hail at the freezing level as

$$N(D) = N_g \exp(-\Lambda_g D) + N_h \exp(-\Lambda_h D) \quad , \quad (2)$$

where subscripts "g" and "h" stand for graupel and hail respectively. The parameters N_g = 8000 m^{-3} mm^{-1} and Λ_g = 1.6 mm^{-1} in (2) are selected in such a way that the "graupel" part of size spectrum yields size distribution of raindrops at the surface which is close to the Marshall – Palmer and the corresponding values of Z and Z_{DR} at S band are 52.2 dBZ and 2.29 dB respectively. These are in agreement with typically observed values of Z and Z_{DR} in heavy rain without hail in Oklahoma (Ryzhkov et al. 2005).

The choice of parameters N_h, Λ_h, and D_{max} (maximal hail size) is dictated by the need to match resulting size distributions of ice cores close to the surface with the observed hail size distributions reported in literature (Ulbrich and Atlas 1982; Cheng and English 1983; Cheng et al. 1985). Here we present results of model simulations for 4 different size distributions at the freezing level as shown in Fig. 4 with the following parameters characterizing distribution of hail aloft

(1) No hail aloft and at the surface (N_h = 0)
(2) Small hail. Hail is present aloft but is totally melted at the surface (D_{max} = 14 mm, Λ_h = 0.99 mm^{-1}, $N_h = 200\Lambda_h^{4.11}$)
(3) Moderate hail. Larger hail aloft with D_{max} = 24 mm so that maximal hail size at the surface is about 19 mm (Λ_h = 0.42 mm^{-1}, $N_h = 400\ \Lambda_h^{4.11}$)
(4) Large hail. D_{max} = 35 mm so that maximal size of hail at the surface is about 30 mm (Λ_h = 0.27 mm^{-1}, $N_h = 800\ \Lambda_h^{4.11}$).

Parameters D_{max} and Λ_h at the freezing level were selected in such a way that the product of their corresponding values at the surface is equal to 7.9 – its most likely value as reported by Ulbrich and Atlas (1982).

Initial bi-exponential size distribution of hydrometeors at the freezing level is modified in the process of melting. As an example, size distributions of graupel / hail at H = 4 km, rain and partially melted hail at H = 0 km, and ice cores at H = 0 km are compared in Fig. 5. Size distribution of rain and melting hail at H = 0 km (thick solid curve) exhibits discontinuity around particle diameter of 8 mm. This is result of shedding. Another consequence of the shedding condition (1) is that hailstones with original sizes between 8 and 14 mm end up as raindrops of the same size of about 8 mm (see Fig. 1) which increases concentration of largest

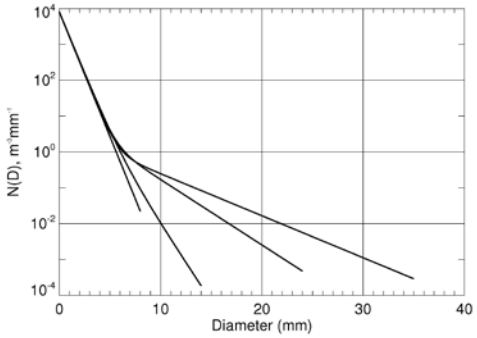

Fig. 4. Examples of graupel / hail size distribution aloft in the cases of no hail, small hail, moderate hail, and large hail for which simulations were made.

raindrops. In reality, such an increase is offset by raindrop breakup. In our Model 1, we eliminate an excess in the number of 8 mm raindrops by spreading water content associated with these drops over the rest of the raindrop spectrum. Note that bi-exponential size distribution of ice particles aloft yields nearly exponential distribution of ice cores (dry graupel and hail) at the surface (dashed line in Fig. 5).

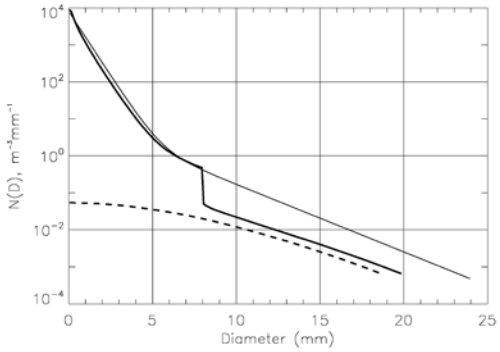

Fig. 5. Size distributions of ice particles at H = 4 km (thin solid line), of raindrops and melting hailstones at H = 0 km (thick solid line), and of ice cores at H = 0 km (dashed lines) in the case when maximal hail size at the surface is ¾ " (19 mm).

5. VERTICAL PROFILES OF RADAR VARIABLES AND THEIR DEPENDENCE ON MAXIMAL HAIL SIZE

.

Vertical profiles of Z, Z_{DR}, A_h, A_{DP}, and K_{DP} simulated at S (λ = 10.97 cm) and C (λ = 5.4 cm) bands corresponding to the cases of no hail, small, moderate, and large hail (as described in the previous section) are displayed in Fig. 6. Thick and thin curves are for C and S band respectively. Blue color denotes no hail, green – small hail, orange – moderate hail, and red – large hail.

As expected, radar reflectivity factor increases with increasing hail size at all heights. Z(S) > Z(C) at higher altitude where drier hail is dominant, whereas Z(S) < Z(C) closer to the surface where the contribution from rain is more significant. Notable is a pronounced maximum in vertical profiles of Z at the height of about 2 km in the cases of moderate and large-size hail. The

increase of Z at the initial stages of melting in the height interval between 2 and 4 km is primarily due to increasing mass water fraction and dielectric constant of melting hailstones. Once melting hailstones start

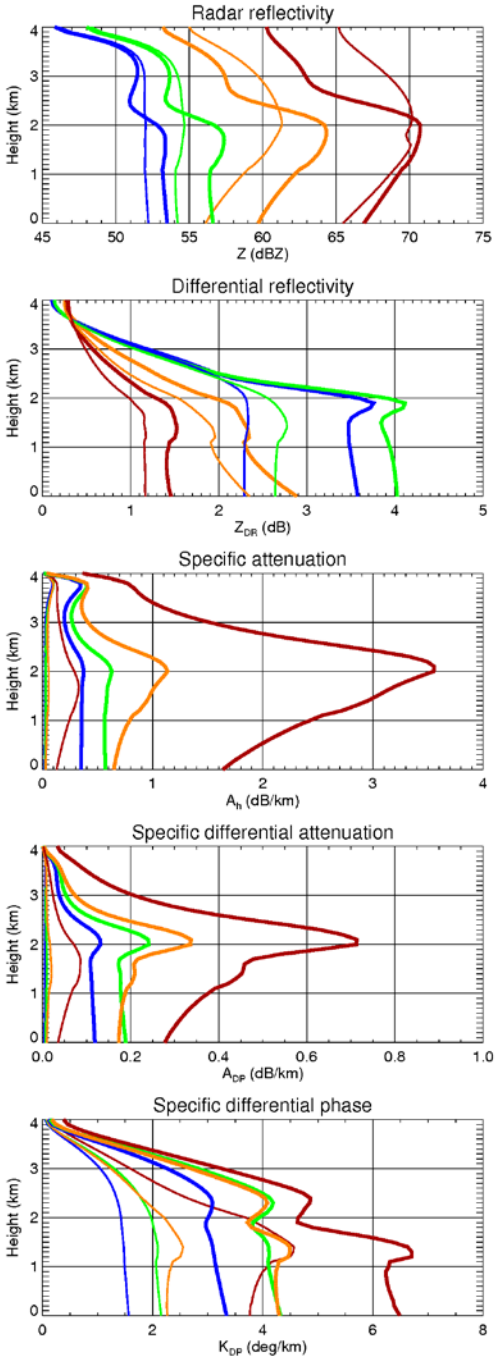

Fig. 6 Vertical profiles of Z_h, Z_{DR}, A_h, A_{DP}, and K_{DP} for the cases of no hail (blue curves), small hail (green curves), moderate hail (orange curves), and large hail (red curves). Thin and thick lines denote profiles at S and C bands respectively.

shedding excessive water (at about 2 km height), their diameters and concentrations (for a given size) decrease (Figs. 1 and 5) resulting in reduction of Z. Such a maximum in the vertical profiles of Z is frequently observed in the radar data collected in hailstorms.

Simulated profiles of differential reflectivity show that Z_{DR} at C band is significantly higher than Z_{DR} at S band below 2 km, where rain contribution to Z_{DR} becomes overwhelming and raindrops with resonance sizes near 6 mm cause Z_{DR} enhancement at C band (see Fig. 3). It is this resonance effect at C band that masks the overall decrease of Z_{DR} due to the presence of hail and affects the quality of polarimetric hail detection at C band (Ryzhkov et al. 2007).

Attenuation parameters A_h and A_{DP} are significantly affected by the presence of melting hail and exhibit well pronounced maxima at the height of about 2 km where shedding starts. This finding is supported by C-band polarimetric observations which frequently exhibit larger differential attenuation at higher antenna elevations within hail-bearing storms (Borowska et al. 2009).

Specific differential phase K_{DP} is a radar parameter which is least affected by melting hail. K_{DP} increases with hail size due to the fact that more hail produces more rain from melt water and it can be shown that vertical profiles of K_{DP} are closely associated with vertical profiles of rain rate (Ryzhkov et al. 2008), thus the R(K_{DP}) rainfall estimator is very efficient in the presence of melting hail.

6. ESTIMATION OF MAXIMAL HAIL SIZE

Relative contributions of rain and melting hail to Z_h, Z_v, A_h, A_{DP}, and K_{DP} at the heights of 0 and 2 km in the case of large hail (with D_{max} = 35 mm at the freezing level) at C band are illustrated in Figs. 7 – 8. At the height of 2 km, hydrometeors contain ice cores if their diameters are larger than 5.7 mm. Fig. 6 shows that these partially melted hailstones with sizes between 5.7 and 25 mm make dominant contributions to all radar variables except K_{DP}. At the surface, i.e., H = 0 km, only particles with D > 8 mm contain ice cores and the contribution of melting hailstones to A_{DP} almost vanishes. However, melting hailstones still contribute significantly to Z_h, Z_v, and A_h along with pure raindrops with D < 8 mm.

Our analysis as well as Fig. 7 and 8 indicate that hailstones larger than 25 – 30 mm contribute very little to all polarimetric variables and smaller size hail with diameters between 10 and 20 mm has biggest impact on all radar variables except K_{DP}. The amount of hail between 10 and 20 mm is determined by the slope Λ_h of hail size distribution and its intercept N_h which can vary almost an order of magnitude for a given Λ_h depending on the temperature of cloud base (Cheng et al. 1985).

Although radar variables are not sensitive to maximal hail size if it exceeds 25 – 30 mm, they are very sensitive to the slope Λ_h which is closely related to D_{max} (Ulbrich and Atlas 1982; Cheng and English 1983), hence D_{max} can be indirectly estimated from Λ_h if the latter one is retrieved from multiparameter radar measurements. Variability in concentration of 10 – 20

mm hailstones for a given Λ_h (or intercept N_h) causes unavoidable uncertainty of such retrievals.

Figs. 9 – 13 illustrate the dependencies of Z, Z_{DR}, A_h, A_{DP}, and K_{DP} at different heights on maximal hail size at the freezing level. Red and blue polygons (for C and S bands correspondingly) show variability of these dependencies if the slope Λ_g changes from 1.6 to 1.7 mm^{-1} and the intercept N_h changes by a factor of 2. Although these plots do not encompass full variability of hail and rain size distributions for a given maximal hail size at the freezing level, they provide some guidance on how to define the parameters of membership functions in the fuzzy logic classification routines for discrimination between small and large hail at S and C band at different heights of the radar sampling volume with respect to the freezing level.

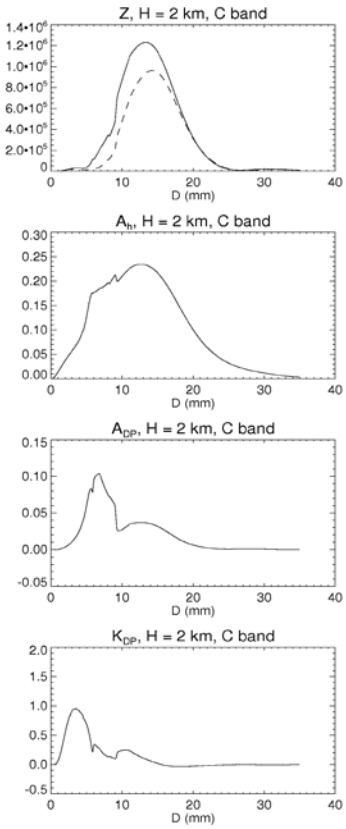

Fig. 7. Relative contributions of different parts of particle size spectrum to C-band Z_h, Z_v (upper panel, dashed line), A_h, A_{DP}, and K_{DP} at the 2 km height in the case of large hail. The y-axis units are arbitrary.

According to the criteria of the US National Weather Service, hail with diameters exceeding ¾" (19 mm) is considered large and hazardous. Hence, the results of simulations for moderate-size hail (24 mm aloft and 19 mm at the surface) can be utilized to determine parameters of the corresponding membership functions.

It is important to realize that such parameters should depend on relative height of the radar resolution volume with respect to the freezing level. Indeed, although diameter of a largest hailstone does not change much as it reaches the surface (from 24 mm to 19 mm), the corresponding radar variables such as Z and Z_{DR} alter significantly as Figs. 9 – 10 show.

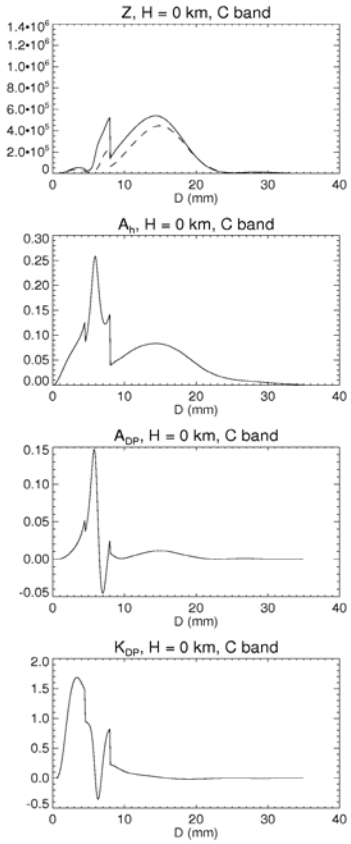

Fig. 8. Same as in Fig. 6, but for the height of 0 km.

Note nonmonotonic behavior of Z_{DR} at lower levels with increasing hail size (Fig. 10). The presence of smaller hail tends to increase Z_{DR} at both radar wavelengths because most of smaller hailstones with initial diameters less than 15 mm melt entirely producing large raindrops with high intrinsic Z_{DR}. Bigger hailstones do not melt completely and offset high Z_{DR} associated with rain part of the size spectrum. This fact also explains the reduction in the difference between Z_{DR} at S and C bands for larger hail sizes.

7. ATTENUATION IN MELTING HAIL

Specific attenuation may increase almost an order of magnitude as maximal hail size changes from 0 to 35 mm. Simulations of C-band A_h using disdrometer data collected in Oklahoma show that it usually does not exceed 0.35 – 0.45 dB/km in rain with reflectivity of 53 dBZ. Recent comparisons of S and C-band reflectivities measured by two closely located radars in Oklahoma revealed C-band A_h within the range between 1 and 3 dB/km in hail-bearing cells with Z > 60 dBZ (Borowska et al. 2009).

Similarly, differential attenuation steadily increases with increasing maximal hail size although at a slower pace compared to A_h. Maximal values of C-band A_{DP} expected in pure rain are between 0.10 and 0.15 dB/km at Z = 53 dBZ, whereas in the presence of hail A_{DP} at C band can be as high as 0.7 – 0.9 dB/km (Borowska et

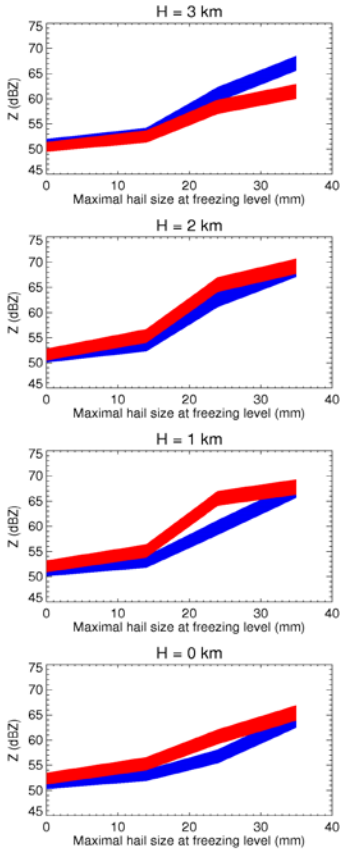

Fig. 9. Dependencies of Z on maximal hail size at the freezing level for variable Λ_g and N_h. It is assumed that $\Lambda_h D_{max}$ = 7.9 (Ulbrich and Atlas 1982). Blue and red polygons depict results of simulations for S and C bands respectively.

al. 2009). The highest magnitudes of A_h and A_{DP} are expected if the center of the radar resolution volume is about 2 km below the freezing level (see also Fig. 6). As Figs. 7 and 8 show, melting hail has greater impact on A_h than on A_{DP}.

Anomalously high attenuation / differential attenuation caused by melting hail pose serious challenge for hail detection and determination of its size. Indeed, radar reflectivity at C band can be negatively biased by more than 10 dB over propagation path of only 2 – 3 km and the corresponding bias in Z_{DR} may exceed 3 – 4 dB (see also Borowska et al. 2009). Attenuation can be significant even at S band. Therefore, reliable hail detection and determination of its size is contingent on accurate correction of Z and Z_{DR} for attenuation.

Polarimetric methods for attenuation correction based on the use of differential phase (e.g., Bringi et al. 1990, 2001; Testud et al. 2000) which were originally

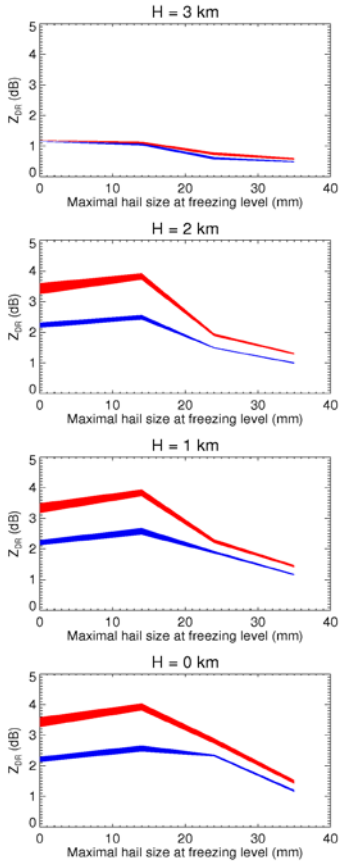

Fig. 10. Same as in Fig. 9 but for Z_{DR}

designed for pure rain assume that the ratios $\alpha = A_h/K_{DP}$ and $\beta = A_{DP}/K_{DP}$ do not change much along the propagation path. This assumption does not hold in the presence of melting hail because K_{DP} is relatively insensitive to hail, whereas A_H and A_{DP} may increase dramatically (especially A_h), hence the ratios α and β are much higher in hail compared to pure rain.

8. SIMULATIONS WITH HUCM MODEL

A hailstorm was simulated with the Model 2 (HUCM) using sounding in southwest Germany on 06/28/2006 (see a more detailed description in Ryzhkov et al. 2009). According to sounding, the height of environmental freezing level was 2.5 km. The Model 2 quite realistically reproduces the pattern of radar reflectivity factor in vertical cross-section, the height of storm top exceeding 12 km, and yields maximal Z of about 65 dBZ at C band in a good agreement with local C-band radar observations.

Simulations with a more sophisticated Model 2 which takes into account all interactions between particles reveal size distributions which may be quite different from the ones assumed in the Model 1. As mentioned earlier, the excess of large raindrops of 8 mm size was artificially eliminated in the Model 1.

Model 2 produces apparent increase in the

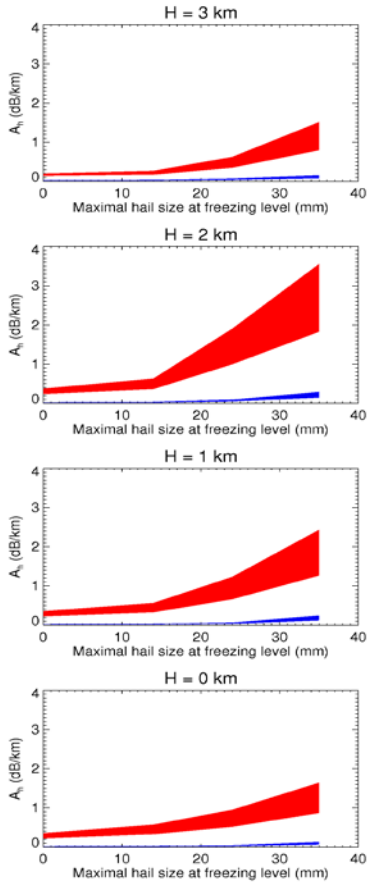

Fig. 11. Same as in Fig. 9 but for A_h.

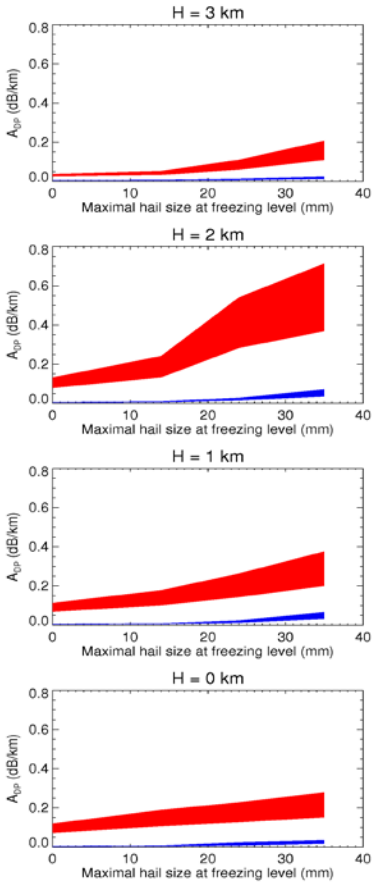

Fig. 12. Same as in Fig. 9 but for A_{DP}

concentration of large raindrops at lower altitudes (Fig. 14). This means that raindrop breakup may not fully offset the influx of largest raindrops due to melting of hailstones with original sizes between 8 and 14 mm. As a result, concentration of largest raindrops is typically higher than the one generated by Model 1 (Fig. 5) and values of Z_{DR} simulated from Model 2 can be noticeably higher than predicted in Model 1 which falls short of producing Z_{DR} of 6 – 7 dB at C band and of 5 dB at S band often observed in severe storms. This can be also partially explained by the fact that simulations by Model 1 in this study do not account for convective updrafts which cause additional size sorting which tends to increase Z_{DR} and decrease ρ_{hv}.

Evolution of size distribution of melting graupel / hail on the way down to the surface simulated by Model 2 is illustrated in Fig. 15. In agreement with Model 1, smaller frozen particles completely melt at lower levels but hail size distribution exhibits well pronounced maximum between 8 and 10 mm diameters. These are partially melted hailstones which affect polarimetric radar variables in the way similar to largest pure raindrops. The concentration of hailstones with such sizes is higher in Model 2 than in Model 1.

An example of the fields of Z and Z_{DR} in vertical cross-section simulated at S and C bands for this hailstorm by the Model 2 is shown in Fig. 16. Two strong convective cells are evident in the RHI plots. The one centered at x = 62 km is associated with descending hail and another one (centered at about 69 km) is in a growing stage. The downdraft is manifested by depression of Z_{DR} below the freezing level (left cell), whereas a Z_{DR} column stretching above freezing level marks location of updraft (right cell). No attenuation effects were simulated in this example.

There are noticeable differences between radar reflectivities at S and C bands due to resonance scattering on large hydrometeors in this case. Most notable, however, is the difference between differential reflectivities. Z_{DR} at C band is significantly higher in the areas of the storm containing either large raindrops or melting hailstones. The corresponding values of the cross-correlation coefficient at C band are also much lower than the ones at S band in these areas (not shown). This is a common pattern routinely observed in real polarimetric data (e.g., Borowska et al. 2009).

Vertical profiles of Z and Z_{DR} at x = 60 km simulated at S and C bands provide a more quantitative measure of such differences (Figs. 17 and 18). Indeed, Z(C) > Z(S) and Z_{DR}(C) > Z_{DR}(S) in full agreement with results of simulations made with the Model 1. However, maximal values of Z_{DR} simulated by the Model 2 are noticeably higher: 6 dB versus 4 dB in Model 1 (see Figs. 6 and 10). Hence, a more realistic Model 2 yields

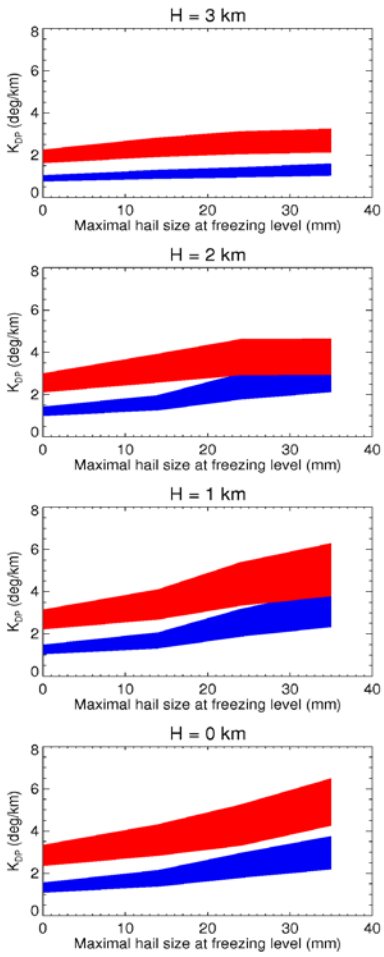

Fig. 13 Same as in Fig. 9 but for K_{DP}.

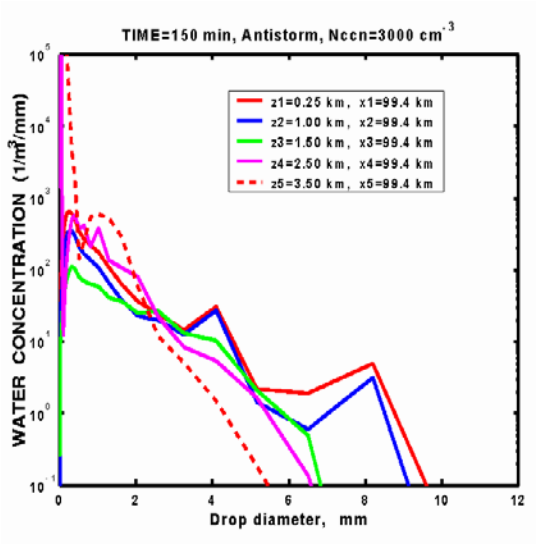

Fig. 14. Size distributions of raindrops at different heights within downdraft associated with hail shaft generated by Model 2 (HUCM).

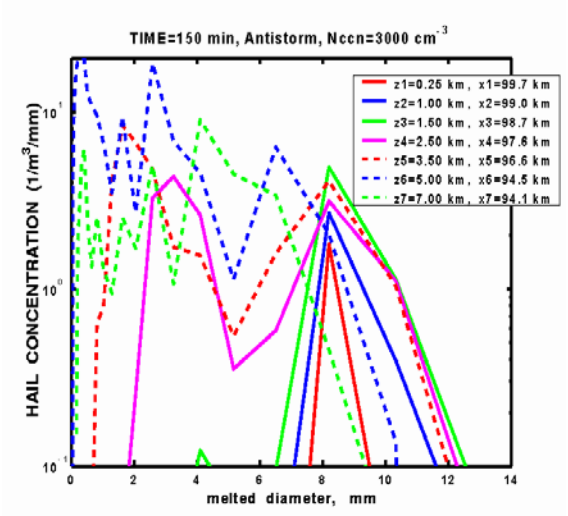

Fig. 15. Size distributions of dry / melting hailstones at different heights within the same hail shaft as in Fig. 14 generated by Model 2 (HUCM).

more realistic maximal values of Z_{DR} (e.g., Ryzhkov et al. 2007; Borowska et al. 2009).

9. CONCLUSIONS

Two cloud models with explicit microphysics have been used to simulate polarimetric signatures of melting hail. One of them (Model 1) is an extension of the 1D Rasmussen – Heymsfield (1987) model of melting hail. Another one (Model 2) is the 2D Hebrew University of Jerusalem cloud model (HUCM) with spectral microphysics. Both models are capable to reproduce realistic values of polarimtric radar variables, their vertical profiles in hailstorms below the freezing level, and to explain significant differences between polarimetric signatures at S and C bands in the storm areas containing large raindrops and melting hailstones.

The dependencies of different polarimetric variables on maximal hail size have been examined which can be utilized for developing classification algorithm for discrimination between smaller and larger hail. It is shown that the parameters of membership functions of such an algorithm crucially depend on the radar wavelength and the height of radar sampling volume with respect to the freezing level.

The Model 1 provides explanation for anomalously high values of specific attenuation A_h and differential attenuation A_{DP} frequently observed in hail-bearing storms. Melting hailstones with sizes between 8 and 20 mm are primarily responsible for high A_h and A_{DP} at higher levels, whereas large raindrops of resonance sizes contribute significantly to A_h and almost exclusively determine A_{DP} at lower heights. Both the presence of melting hail of moderate size and the increase in concentration of largest raindrops originated from melting hail may cause very strong attenuation effects at C band.

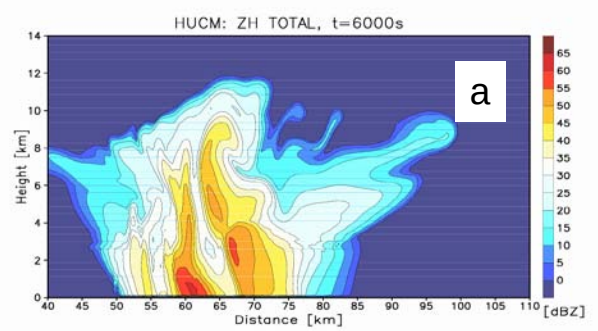

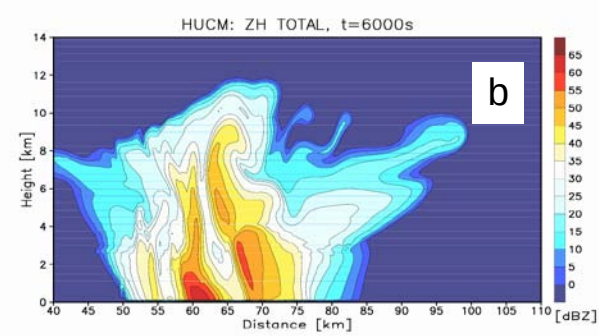

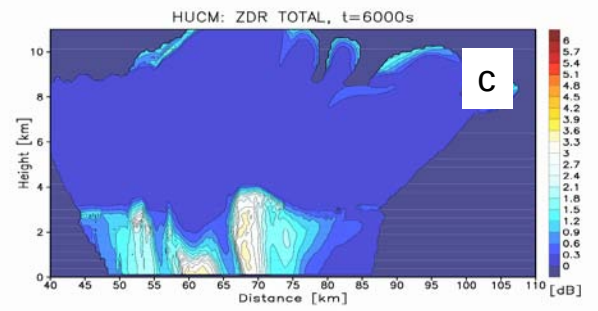

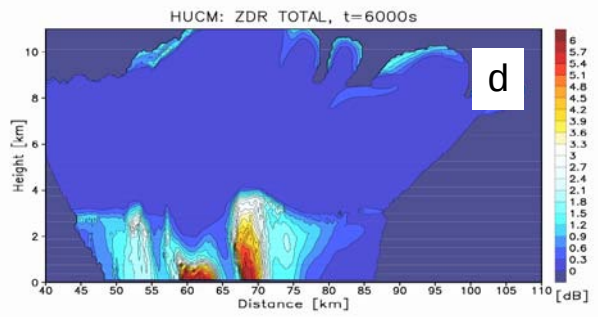

Fig. 16. RHIs of Z and Z_{DR} at S (a,c) and C (b,d) bands in hailstorm simulated by Model 2 (HUCM) (Ryzhkov et al. 2009).

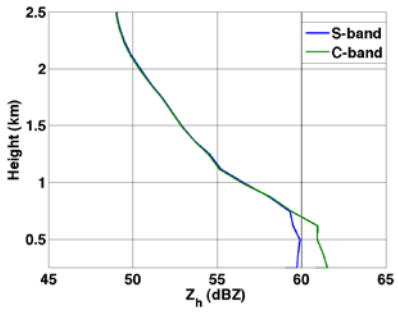

Fig. 17. Vertical profiles of Z at S and C bands simulated by Model 2 (HUCM) in the downdraft area containing hail at x = 60 km in Fig. 16.

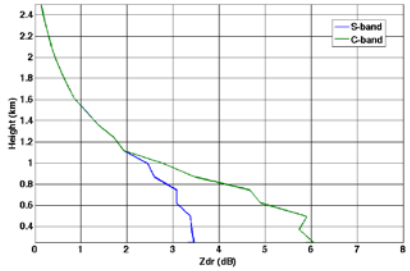

Fig. 18. Same as in Fig. 17 but for Z_{DR}.

REFERENCES

Aydin, K., and Y. Zhao, 1990: A computational study of polarimetric radar observables in hail. *IEEE Trans. Geosci. Rem. Sens.*, **28**, 412 – 422.

Aydin, K., and V. Giridhar, 1991: Polarimetric C-band radar observables in melting hail: a computational study. Preprints. *25th Int. Conf. Radar Meteor*. Paris, 733 – 736.

Borowska, L., A. Ryzhkov, D. Zrnic, J.-Y. Gu, P. Neilley, M. Knight, R. Palmer, B. Cheong, C. Simmer, 2009: Attenuation of radar signal in melting hail at C band. *Extended Abstracts, 34 Conf. Radar Meterol.,* Williamsburg, VA, P2.7.

Bringi, V., and V. Chandrasekar, 2001: *Polarimetric Doppler Weather Radar. Principles and Applications.* Cambridge University Press, 636 pp.

Bringi, V. N., V. Chandrasekar, N. Balakrishnan, and D. S. Zrnic, 1990: An examination of propagation effects in rainfall on polarimetric variables at microwave frequencies. *J. Atmos. Oceanic Technol.*, **7**, 829-840.

Bringi, V. N., T. D. Keenan, and V. Chandrasekar, 2001: Correcting C-band radar reflectivity and differential reflectivity data for rain attenuation: A self-consistent method with constraints. *IEEE Trans. Geosci. Remote Sens.*, **39**, 1906-1915.

Cheng, L., and M. English, 1983: A relationship between

hailstone concentration and size. *J. Atmos. Sci.*, **40**, 204 – 213.

Cheng, L., M. English, and R. Wong, 1985: Hailstone size distributions and their relationship to storm thermodynamics. *J. Clim. Appl. Meteor*., **24**, 1059 – 1067.

Depue, T., P. Kennedy, and S. Rutledge, 2007: Performance of the hail differential reflectivity (H_{DR}) polarimetric hail indicator. *J. Appl. Meteor.Clim*., **46**, 1290 – 1301.

Heinselman, P., and A. Ryzhkov, 2006: Validation of polarimetric hail detection. *Wea. Forecasting*, **21**, 839 – 850.

Khain, A., A. Pokrovsky, M. Pinsky, A. Seifert, and V. Phillips, 2004: Effects of atmospheric aerosols on deep convective clouds as seen from simulations using a spectral microphysics mixed-phase cumulus cloud model. Part I: Model description. *J. Atmos. Sci.*, **61**, 2963 – 2982.

Kumjian, M., and A. Ryzhkov, 2008: Interpretation of polarimetric signatures in supercell storms using explicit microphysical modeling. *Extended Abstracts, 5th European Conference on Radar in Meteorology and Hydrology*, Helsinki, Finland, CD-ROM, P7.2.

Park., H.-S., A. Ryzhkov, D. Zrnic, and K.E. Kim, 2009: The hydrometeor classification algorithm for polarimetric WSR-88D. Description and application to an MCS. *Wea. Forecasting*, **24**, 730 – 748.

Rasmussen, R., and J. Heymsfield, 1987: Melting and shedding of graupel and hail. Part I: Model physics. *J. Atmos. Sci.*, **44**, 2754 – 2763.

Ryzhkov, A.V., S.E. Giangrande, V. M. Melnikov, and T.J. Schuur, 2005: Calibration issues of dual-polarization radar measurements. *J. Atmos. Oceanic Technol.,* **22**, 1138 -1155.

Ryzhkov, A., D. Zrnic, P. Zhang, J. Krause, H. Park, D. Hudak, J. Young, J. Alford, M. Knight, and J. Conway, 2007: Comparison of polarimetric algorithms for hydrometeor classification at S and C bands. Analysis of the performance in different climate regions. *33 Conf. Radar Meteor*., Cairns, Australia, CD-ROM 10.3.

Ryzhkov, A., S. Giangrande, A. Khain, M. Pinsky, and A. Pokrovsky, 2008: Exploring model-based polarimetric retrieval of vertical profiles of precipitation. *5th European. Conf. Radar Meteor. Hydrol.*, Helsinki, Finland, CD ROM, P6.1.

Ryzhkov, A., M. Pinsky, A. Pokrovsky, and A. Khain, 2009: Polarimetric radar observation operator for a cloud model with spectral microphysics. Submitted to *J. Appl. Meteor.*

Smith, P., D. Musil, S. Weber, J. Spahn, G. Johnson, and W. Sand, 1976: Raindrop and hailstone distributions inside hailstorms. Preprints. *Int. Conf. Cloud Physics*, Boulder, CO, 252 – 257.

Spahn, J. and P. Smith, 1976: Some characteristics of hailstone size distributions inside hailstorms. Preprints, *17th Conf. Radar Meteor.*, Seattle, WA, 187 – 191.

Tabary, P., G. Vulpiani, J. J. Gourley, A. J. Illingworth and O. Bousquet, 2008: Unusually large attenuation at C-band in Europe: How often does it happen? What is the origin? Can we correct for it? *Fifth European Conference on Radar in Meteorology and Hydrology. Helsinki, Finland, 30 Jun. – 4 Jul.*

Testud, J., E. Le Bouar, E. Obligis, and M. Ali-Mehenni, 2000: The rain profiling algorithm applied to polarimetric weather radar. *J. Atmos. Oceanic Technol.*, **17**, 332-456.

Ulbrich, C. and D. Atlas, 1982: Hail parameter relations: a comprehensive digest. *J. Appl. Meteor.*, **21**, 22 – 43.

Vivekanandan, J., V. Bringi, and R. Raghavan, 1990: Multiparameter radar modeling and observation of melting ice, *J. Atmos. Sci.*, **47**, 549 – 563.